Computation of transient viscous flows using indirect radial basis function networks

N. Mai-Duy[1], L. Mai-Cao[2] and T. Tran-Cong[3]

Abstract: In this paper, an indirect/integrated radial-basis-function network (IRBFN) method is further developed to solve transient partial differential equations (PDEs) governing fluid flow problems. Spatial derivatives are discretized using one- and two-dimensional IRBFN interpolation schemes, whereas temporal derivatives are approximated using a method of lines and a finite-difference technique. In the case of moving interface problems, the IRBFN method is combined with the level set method to capture the evolution of the interface. The accuracy of the method is investigated by considering several benchmark test problems, including the classical lid-driven cavity flow. Very accurate results are achieved using relatively low numbers of data points.

Keyword: indirect radial basis function networks, integrated radial basis function networks, transient viscous flow

1 Introduction

The idea of using RBFNs for solving PDEs was first proposed by Kansa (1990), where a global multiquadric scheme was used in conjunction with point collocation to discretize parabolic, hyperbolic and elliptic PDEs. The RBF methods rely on a set of random points, rather than a set of finite elements, to discretize the PDEs and the field variables. For certain values of RBF widths, the methods are capable of giving very accurate results. These features make the RBF methods very attractive. They have found applications in many branches of computational engineering, for example, in heat transfer [e.g. La-Rocca, Power, La-Rocca, and Morale (2005)], fluid flow [e.g. Mai-Duy (2004); Sarler (2005); Shu, Ding, and Yeo (2005); Chantasiriwan (2006)], solid mechanics [e.g. Tolstykh and Shirobokov (2005)], micro-electrical-mechanical system [e.g. Hon, Ling, and Liew (2005)] and electromagnetism [e.g. Young, Chen, and Wong (2005)]. Recently, Mai-Duy and Tran-Cong (2001a), Mai-Duy and Tran-Cong (2001b), Mai-Duy and Tran-Cong (2003), Mai-Duy and Tran-Cong (2005) proposed an indirect RBFN method, which is based on integration rather than differentiation, for approximating functions and their derivatives and for solving elliptic differential equations. In Kansa method, a function is first approximated by an RBFN, and its derivatives are then obtained by differentiating such an RBFN. In the IRBFN method, on the other hand, the highest-order derivatives in the system under consideration are first decomposed into RBFs. Lower-order derivatives and the function itself are then successively obtained via symbolic integrations. More recently, Mai-Cao and Tran-Cong (2005) extended the IRBFN method for solving transient problems governed by parabolic, hyperbolic and convection-diffusion equations. This paper reports further developments of the IRBFN method to solve transient PDEs governing viscous flow problems. Several interpolation schemes based on 1D− and 2D−IRBFNs are employed to approximate spatial derivatives, whereas a semi-

---

[1] CESRC, Faculty of Engineering and Surveying, University of Southern Queensland, Toowoomba Qld 4350, Australia.

[2] CESRC, Faculty of Engineering and Surveying, University of Southern Queensland, Toowoomba Qld 4350, Australia. Current address: Department of Geology & Petroleum Engineering, Ho Chi Minh City University of Technology, 268 Ly Thuong Kiet, Q.10, Ho Chi Minh City, Vietnam

[3] CESRC, Faculty of Engineering and Surveying, University of Southern Queensland, Toowoomba Qld 4350, Australia, email: trancong@usq.edu.au, Fax: +61 7 46312526.

discrete scheme/a method of lines [e.g. Mai-Cao and Tran-Cong (2005)] and a finite-difference technique are used for temporal discretization. For problems with moving interfaces, the present method is combined with the level set method to capture the evolution of interfaces. A number of benchmark test problems, namely a convection-diffusion problem governed by the Burgers equation, the lid-driven cavity flow governed by the Navier-Stokes equations, and passive transport problems governed by hyperbolic equations, are considered. These problems have received much attention from the research community. The first two problems are usually used as models for the understanding of physical flows and for the testing of new numerical schemes in CFD, while the last problem presents several challenges associated with the moving interfaces.

A distinguish feature of the Burgers equation is that it can be solved analytically for many combinations of initial and boundary conditions [Fletcher (1984)] and hence, one can evaluate the accuracy of a numerical method in a straightforward manner. In contrast, there are no exact solutions available for the others. The lid-driven cavity flow possesses physically unrealistic characteristics (discontinuous velocity) at the edges of the lid. This leads to rapid changes in stress near those points, thereby making the numerical simulation difficult. In the context of a Newtonian-fluid flow, accurate solutions for a wide range of the Reynolds number were reported by Ghia, Ghia, and Shin (1982) who used a multigrid finite-difference (FD) scheme with very dense grids, and their results are often cited in the literature for evaluating new viscous flow solvers. Recently, by using the Chebyshev collocation technique, which possesses exponential convergence/spectral accuracy, for the calculation of a regular part of the solution, and by using analytical formulae to obtain the singular part, Botella and Peyret (1998) provided benchmark spectral results on the flow at Re=1000. It will be shown that the 1D-IRBFN results are in closer agreement with the spectral solutions than the FD ones. For moving interface problems, there are two basic approaches to model the movement of the interfaces: moving-

grid and fixed-grid methods. In the moving-grid methods, the interface is treated as the boundary of a moving surface-fitted grid. This approach allows a precise representation of the interface whereas its main drawback is the severe deformation of the mesh as the interface moves. The second approach, which is based on fixed grids, includes capturing methods where the moving interface is not explicitly tracked, but rather captured via a characteristic function. For these methods, no grid manipulation (e.g. rezoning/remeshing) is needed to maintain the overall accuracy even when the interface undergoes large deformation. Interested readers are referred to [e.g. Floryan and Rasmussen (1989)] for a thorough review of numerical methods for moving interfaces. In this paper, the level set method, which belongs to fixed-grid methods, is used to capture the moving interfaces.

The remaining of the paper is organized as follows. In section 2, the IRBFN method for solving time-dependent PDEs is described. The method is then applied to simulate convection-diffusion, lid-driven cavity flow, and moving interface problems in sections 3, 4 and 5, respectively. Section 6 gives some concluding remarks.

2 Indirect RBFN method

2.1 *Spatial discretization*

A function y, to be approximated, can be represented by an RBFN as

$$y(\mathbf{x}) \approx f(\mathbf{x}) = \sum_{i=1}^{M} w^{(i)} g^{(i)}(\mathbf{x}), \qquad (1)$$

where $\mathbf{x}$ is the input vector, M the number of RBFs, $\{w^{(i)}\}_{i=1}^{M}$ the set of network weights to be found, and $\{g^{(i)}(\mathbf{x})\}_{i=1}^{M}$ the set of RBFs.

In the present indirect approach, RBFNs are used to represent the second-order derivatives of a function y, i.e. $\partial^2 y/\partial x_1^2$ and $\partial^2 y/\partial x_2^2$. Lower-order derivatives and the function itself are then obtained by integrating those RBFNs.

2.1.1 Expressions in terms of network weights

Expressions of f and its derivatives in terms of network weights can be given by

$$\frac{\partial^2 y(\mathbf{x})}{\partial x_j^2} \approx \frac{\partial^2 f(\mathbf{x})}{\partial x_j^2} = \sum_{i=1}^{M} w_{[x_j]}^{(i)} g_{[x_j]}^{(i)}(\mathbf{x}), \tag{2}$$

$$\frac{\partial y(\mathbf{x})}{\partial x_j} \approx \frac{\partial f(\mathbf{x})}{\partial x_j} = \int \left(\sum_{i=1}^{M} w_{[x_j]}^{(i)} g_{[x_j]}^{(i)}(\mathbf{x}) \right) dx_j$$

$$= \sum_{i=1}^{M+P} w_{[x_j]}^{(i)} H_{[x_j]}^{(i)}(\mathbf{x}), \tag{3}$$

$$y(\mathbf{x}) \approx f_{[x_j]}(\mathbf{x}) = \int \left(\sum_{i=1}^{M+P} w_{[x_j]}^{(i)} H_{[x_j]}^{(i)}(\mathbf{x}) \right) dx_j$$

$$= \sum_{i=1}^{M+Q} w_{[x_j]}^{(i)} \overline{H}_{[x_j]}^{(i)}(\mathbf{x}), \tag{4}$$

where subscript $[x_j]$ denotes the quantities resulting from the process of integration with respect to the x_j- direction, and P and Q are the numbers of centres used to represent integration constants in the first and second derivatives, respectively ($Q = 2P$). Let $\{\mathbf{x}^{(i)}\}_{i=1}^{N}$ be the set of collocation points. If the above expressions are evaluated at the chosen collocation points, one would obtain a discrete system in terms of network weights. More details can be found in [Mai-Duy and Tran-Cong (2001a), Mai-Duy and Tran-Cong (2001b), Mai-Duy and Tran-Cong (2003)].

2.1.2 Expressions in terms of nodal function values

As an alternative approach, further manipulation of the discrete system is carried out to convert the system into the unknown function values at collocation points. Thus, expressions of f and its derivatives in terms of function values can be

given by

$$\frac{\partial^2 f(\mathbf{x})}{\partial x_j^2} = \left[g_{[x_j]}^{(1)}(\mathbf{x}), \cdots, 0, \cdots, 0, \cdots \right] \overline{\mathbf{H}}_{[x_j]}^{-1} \mathbf{f}, \tag{5}$$

$$\frac{\partial f(\mathbf{x})}{\partial x_j} = \left[H_{[x_j]}^{(1)}(\mathbf{x}), \cdots, H_{[x_j]}^{(M+1)}(\mathbf{x}), \right.$$
$$\left. \cdots, 0, \cdots \right] \overline{\mathbf{H}}_{[x_j]}^{-1} \mathbf{f}, \tag{6}$$

$$f_{[x_j]}(\mathbf{x}) = \left[\overline{H}_{[x_j]}^{(1)}(\mathbf{x}), \cdots, \overline{H}_{[x_j]}^{(M+1)}(\mathbf{x}), \right.$$
$$\left. \cdots, \overline{H}_{[x_j]}^{(M+P+1)}(\mathbf{x}), \cdots \right] \overline{\mathbf{H}}_{[x_j]}^{-1} \mathbf{f}, \tag{7}$$

where $\mathbf{f}$ is the vector of unknown function values at the collocation points, and $\overline{\mathbf{H}}_{[x_j]}$ is the conversion matrix defined as

$$\overline{\mathbf{H}}_{[x_j]} = \begin{bmatrix} \overline{H}_{[x_j]}^{(1)}(\mathbf{x}^{(1)}), & \cdots, & \overline{H}_{[x_j]}^{(M+1)}(\mathbf{x}^{(1)}), \\ \overline{H}_{[x_j]}^{(1)}(\mathbf{x}^{(2)}), & \cdots, & \overline{H}_{[x_j]}^{(M+1)}(\mathbf{x}^{(2)}), \\ \cdots & \cdots & \cdots \\ \overline{H}_{[x_j]}^{(1)}(\mathbf{x}^{(N)}), & \cdots, & \overline{H}_{[x_j]}^{(M+1)}(\mathbf{x}^{(N)}), \\ & \cdots, & \overline{H}_{[x_j]}^{(M+P+1)}(\mathbf{x}^{(1)}), & \cdots \\ & \cdots, & \overline{H}_{[x_j]}^{(M+P+1)}(\mathbf{x}^{(2)}), & \cdots \\ & \cdots & \cdots & \cdots \\ & \cdots, & \overline{H}_{[x_j]}^{(M+P+1)}(\mathbf{x}^{(N)}), & \cdots \end{bmatrix}.$$

More details can be found in [Mai-Duy and Tran-Cong (2005)].

It can be seen that the 2D$-$IRBFN expressions (5)-(7) require the inversion of large non-square matrices $\overline{\mathbf{H}}_{[x_j]}$ of dimension $N \times (M+Q)$. To alleviate this difficulty, one can discretize the domain of interest using a Cartesian grid, and then apply 1D$-$IRBFNs to represent the variations of the variable and its derivative along grid lines. In this case, the inversion is conducted for a series of much smaller matrices,

$$\overline{\mathbf{H}}_{[x_j]} = \begin{bmatrix} \overline{H}_{[x_j]}^{(1)}(x_j^{(1)}) & \overline{H}_{[x_j]}^{(2)}(x_j^{(1)}) \\ \overline{H}_{[x_j]}^{(1)}(x_j^{(2)}) & \overline{H}_{[x_j]}^{(2)}(x_j^{(2)}) \\ \cdots & \cdots \\ \overline{H}_{[x_j]}^{(1)}(x_j^{(n)}) & \overline{H}_{[x_j]}^{(2)}(x_j^{(n)}) \\ \cdots & \overline{H}_{[x_j]}^{(n)}(x_j^{(1)}) & x_j^{(1)} & 1 \\ \cdots & \overline{H}_{[x_j]}^{(n)}(x_j^{(2)}) & x_j^{(2)} & 1 \\ \cdots & \cdots & \cdots & \cdots \\ \cdots & \overline{H}_{[x_j]}^{(n)}(x_j^{(n)}) & x_j^{(n)} & 1 \end{bmatrix},$$

of dimension $n \times (n+2)$ in which n is the number of data points along a grid line that is parallel to the x_j- direction. This leads to considerable economy in forming the system matrix over the use of 2D-IRBFNs. As a result, much larger numbers of nodes (e.g., up to 10201 nodes in this study) can be employed. This approach is recommended for solving complex problems, such as the lid-driven cavity flow problem, where a number of data points is required to be large enough in order to capture complex flow patterns.

For all numerical examples, the multiquadric function is utilized and hence the basis function g takes the form

$$g^{(i)}(\mathbf{x}) = \sqrt{\|\mathbf{x} - \mathbf{c}^{(i)}\|^2 + a^{(i)2}}, \qquad (8)$$

where $\mathbf{c}$ is the centre, a is the width and $\|.\|$ denotes a Euclidean norm. The set of collocation points is taken to be the set of centres, i.e. $\{x^{(i)}\}_{i=1}^{N} \equiv \{c^{(i)}\}_{i=1}^{M}$ with $N = M$, and the width $a^{(i)}$ is chosen to be the minimum distance from the ith centre to its neighbours.

2.2 Temporal discretization

For problems governed by the Burgers equation and the Navier-Stokes equations, a finite-difference scheme is used for temporal discretization, where the diffusive and convective terms are treated implicitly and explicitly, respectively.

For moving interface problems, a method of lines is employed. The numerical solution of the ODE system resulting from the semi-discretization of the PDE is found by means of the fourth-order Runge-Kutta method.

3 Convection-diffusion problem

Consider a convection-diffusion problem governed by the Burgers equation. The purpose of giving this example here is to illustrate the ability of the present method to capture sharp gradients accurately. The method can then be used with confidence to solve more complex problems. The Burger equation is defined as follows.

$$\frac{\partial u}{\partial t} + u\frac{\partial u}{\partial x} = \frac{1}{Re}\frac{\partial^2 u}{\partial x^2}, \quad x \in \Omega = [-1, 1], \qquad (9)$$

with boundary conditions

$$u(-1,t) = 1, \quad u(1,t) = 0, \qquad (10)$$

and initial conditions

$$u_0(x) = u(x,0) = 1, \quad -1 \le x \le 0, \qquad (11)$$

$$u_0(x) = u(x,0) = 0, \quad 0 < x \le 1, \qquad (12)$$

where u is velocity, and Re the Reynolds number. Since it is a 1D problem, the differential equation can be solved efficiently, without the need for converting RBF coefficients into nodal values. The IRBFN expressions (2)-(4) can thus be used to represent the variable and its derivatives. The space domain is discretised with 101 collocation points. Results for the cases $Re = 10$ and $Re = 100$ are shown in Figure 1 where excellent agreement with the exact solution [Fletcher (1984)] can be seen. The "shock" front becomes diffused at low Re values and remains steep with increasing Re values.

4 Lid-driven cavity flow

This is a classical benchmark problem which is suitably used here to demonstrate the capability of the present method to simulate complex fluid flows. The lid velocity (U) and the length of the side of the square (L) are used as reference quantities. The non-dimensional governing equations for unsteady two-dimensional incompressible flow of a Newtonian fluid in terms of the streamfunction ψ and vorticity ω can be written as follows

$$\frac{\partial \omega}{\partial t} + \left(\frac{\partial \psi}{\partial x_2}\frac{\partial \omega}{\partial x_1} - \frac{\partial \psi}{\partial x_1}\frac{\partial \omega}{\partial x_2}\right)$$
$$= \frac{1}{Re}\left(\frac{\partial^2 \omega}{\partial x_1^2} + \frac{\partial^2 \omega}{\partial x_2^2}\right), \quad (13)$$

$$\frac{\partial^2 \psi}{\partial x_1^2} + \frac{\partial^2 \psi}{\partial x_2^2} = -\omega, \qquad (14)$$

where $Re = UL/\nu$ is the Reynolds number(ν: the kinematic viscosity). The vorticity and streamfunction are defined by

$$\omega = \frac{\partial v_2}{\partial x_1} - \frac{\partial v_1}{\partial x_2}, \qquad (15)$$

$$\frac{\partial \psi}{\partial x_1} = -v_2, \quad \frac{\partial \psi}{\partial x_2} = v_1, \qquad (16)$$
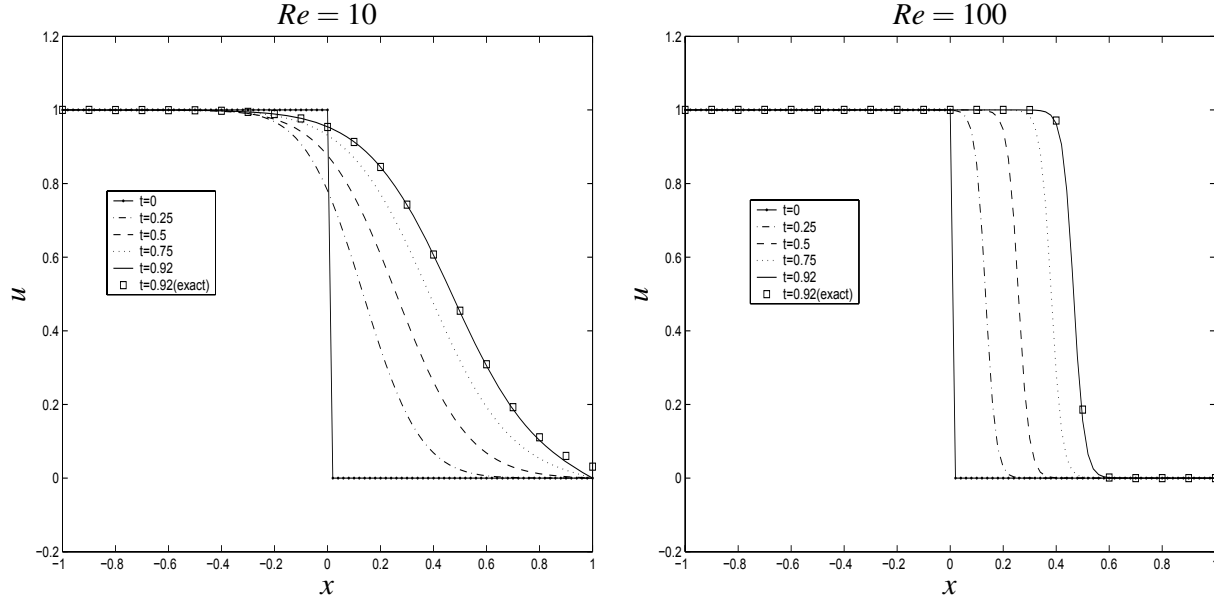
Figure 1: Burgers equation, 101 data points, $\Delta t = 0.001$: the evolution of the "shock" front.

where v_1 and v_2 are two components of the velocity vector in the x_1- and x_2-directions, respectively.

The lid slides toward the right at unit velocity, while the other walls remain stationary:

$$\psi = 0, \quad \frac{\partial \psi}{\partial x_1} = 0, \quad \text{on} \quad x_1 = 0 \text{ and } x_1 = 1, \quad (17)$$

$$\psi = 0, \quad \frac{\partial \psi}{\partial x_2} = 0, \quad \text{on} \quad x_2 = 0, \quad (18)$$

$$\psi = 0, \quad \frac{\partial \psi}{\partial x_2} = 1, \quad \text{on} \quad x_2 = 1. \quad (19)$$

The boundary condition $\psi = 0$ along the boundaries can be used directly to solve (14) for the velocity field, while one needs to derive computational boundary conditions for the vorticity transport equation (13). Using (14) and the boundary condition $\psi = 0$, expressions for the vorticity on the boundaries are reduced to $\omega = -\partial^2 \psi / \partial n^2$ (n: the local coordinate normal to the wall). After expressing this normal second-order derivative as a linear combination of nodal first-order derivative values, imposition of the required boundary conditions $\partial \psi / \partial n$ is carried out. Finally, the remaining first derivative values are written in terms of nodal streamfunction values. This process is similar to that of a 2D-IRBFN interpolation scheme which was described in detail in [Mai-Duy and

Tran-Cong (2005)]. The present solution procedure involves the following steps

1. Guess a set of initial conditions: ω, ψ and their spatial derivatives

2. Discretize in time using a finite-difference scheme,

3. Discretize in space using 1D-IRBFN schemes:
   Compute the convective term and the boundary values of ω
   Solve the vorticity transport equation (13) for ω
   Solve Poisson equation (14) for ψ

4. Check to see whether the solution has reached a steady state

$$\frac{\sqrt{\sum_{i=1}^{N} \left(\psi_{k+1}^{(i)} - \psi_k^{(i)} \right)^2}}{\sqrt{\sum_{i=1}^{N} \left(\psi_{k+1}^{(i)} \right)^2}} < \varepsilon, \quad (20)$$

where k is the time level, ε the tolerance ($\varepsilon = 10^{-9}$), and N the number of collocation points.

5. If it is not satisfied, advance time step and repeat from step 2. Otherwise, stop the computation and output the results.

Table 1: Lid-driven cavity flow, $Re = 100$: Extrema of the vertical and horizontal velocity profiles through the centre of the cavity.

Method	Density	v_{1min}(error %)	x_2	v_{2max}(error %)	x_1	v_{2min}(error %)	x_1
Present	11×11	-0.18388(14.091)	0.484	0.14175(21.061)	0.242	-0.20870(17.770)	0.814
	21×21	-0.21085(1.490)	0.464	0.17450(2.823)	0.239	-0.24734(2.545)	0.808
	31×31	-0.21367(0.173)	0.459	0.17895(0.345)	0.237	-0.25278(0.402)	0.810
	41×41	-0.21408(0.019)	0.458	0.17960(0.017)	0.237	-0.25368(0.047)	0.810
FVM [Deng, Piquet, Queutey, and Visonneau (1994)]	64×64	-0.21315(0.416)	—	0.17896(0.340)	—	-0.25339(0.162)	—
FDM($\psi - \omega$) [Ghia, Ghia, and Shin (1982)]	129×129	-0.21090(1.467)	0.453	0.17527(2.395)	0.234	-0.24533(3.337)	0.805
FDM($\mathbf{u} - p$) [Bruneau and Jouron (1990)]	129×129	-0.2106 (1.607)	0.453	0.1786 (0.540)	0.234	-0.2521 (0.670)	0.813
Benchmark [Botella and Peyret (1998)]		-0.21404	0.458	0.17957	0.237	-0.25380	0.810

Table 2:: Lid-driven cavity flow, $Re = 1000$: Extrema of the vertical and horizontal velocity profiles through the centre of the cavity. Note that cpi.: consistent physical interpolation; stagg.: staggered.

Method	Density	v_{1min}(error %)	x_2	v_{2max}(error %)	x_1	v_{2min}(error %)	x_1
Present	11×11	-0.16933(56.422)	0.244	0.14892(60.492)	0.218	-0.20926(60.298)	0.906
	21×21	-0.28334(27.081)	0.254	0.25166(33.236)	0.185	-0.35962(31.771)	0.875
	31×31	-0.33588(13.560)	0.192	0.32263(14.408)	0.167	-0.46097(12.543)	0.891
	41×41	-0.36667(5.636)	0.177	0.35368(6.171)	0.163	-0.49844(5.434)	0.903
	51×51	-0.37859(2.568)	0.174	0.36588(2.934)	0.161	-0.51356(2.565)	0.907
	61×61	-0.38300(1.434)	0.174	0.37060(1.682)	0.160	-0.51939(1.459)	0.908
	71×71	-0.38496(0.929)	0.173	0.37279(1.101)	0.159	-0.52199(0.966)	0.908
	81×81	-0.38603(0.654)	0.173	0.37403(0.772)	0.159	-0.52344(0.691)	0.909
	91×91	-0.38671(0.479)	0.173	0.37482(0.562)	0.159	-0.52436(0.516)	0.909
	101×101	-0.38717(0.360)	0.172	0.37536(0.419)	0.158	-0.52499(0.397)	0.909
FVM,stagg.	128×128	-0.38050(2.077)	—	0.36884(2.149)	—	-0.51727(1.861)	—
FVM,cpi.	128×128	-0.38511(0.890)	—	0.37369(0.862)	—	-0.52280(0.812)	—
[Deng, Piquet, Queutey, and Visonneau (1994)]							
FDM($\psi - \omega$)	129×129	-0.38289(1.462)	0.172	0.37095(1.589)	0.156	-0.51550(2.197)	0.906
[Ghia, Ghia, and Shin (1982)]							
FDM($\mathbf{u} - p$)	256×256	-0.3764 (3.132)	0.160	0.3665 (2.770)	0.152	-0.5208 (1.192)	0.910
[Bruneau and Jouron (1990)]							
Benchmark		-0.38857	0.172	0.37694	0.158	-0.52708	0.909
[Botella and Peyret (1998)]							

Table 3: Lid-driven cavity flow, $Re = 1000$, Primary vortex: Intensities. The results obtained by the spectral method and FDM are also included for comparison.

Method	Density	ψ_{min}(error %)	ω(error %)	x_1	x_2
Present	11×11	-0.05733(51.799)	-1.02512(50.423)	0.574	0.581
	21×21	-0.08417(29.233)	-1.66318(19.566)	0.534	0.601
	31×31	-0.10317(13.259)	-1.87115(9.508)	0.530	0.572
	41×41	-0.11242(5.482)	-1.98425(4.038)	0.532	0.566
	51×51	-0.11594(2.522)	-2.03170(1.743)	0.532	0.566
	61×61	-0.11727(1.404)	-2.04909(0.902)	0.531	0.566
	71×71	-0.11787(0.900)	-2.05637(0.550)	0.531	0.566
	81×81	-0.11819(0.631)	-2.06013(0.369)	0.531	0.566
	91×91	-0.11840(0.454)	-2.06237(0.260)	0.531	0.566
	101×101	-0.11854(0.336)	-2.06396(0.183)	0.531	0.565
FDM($\psi - \omega$) [Ghia, Ghia, and Shin (1982)]	129×129	-0.11793(0.849)	-2.04968(0.874)	0.531	0.563
FDM($\mathbf{u} - p$) [Bruneau and Jouron (1990)]	256×256	-0.1163 (2.220)	—	0.531	0.559
Benchmark [Botella and Peyret (1998)]	—	-0.11894	-2.06775	0.531	0.565

Table 4: Lid-driven cavity flow, $Re = 1000$, lower right secondary vortex: Intensities. The results obtained by the spectral method and FDM are also included for comparison.

Method	Density	ψ_{max}(error %)	ω(error %)	x_1	x_2
Present	21×21	0.00330(90.751)	1.02999(7.191)	0.806	0.156
	41×41	0.00170(1.734)	1.03920(6.361)	0.863	0.115
	61×61	0.00175(1.156)	1.09919(0.955)	0.863	0.113
	81×81	0.00175(1.156)	1.10692(0.259)	0.863	0.112
	101×101	0.00174(0.578)	1.10860(0.107)	0.864	0.112
FDM($\psi - \omega$) [Ghia, Ghia, and Shin (1982)]	129×129	0.00175(1.156)	1.15465(4.042)	0.859	0.109
FDM($\mathbf{u} - p$) [Bruneau and Jouron (1990)]	256×256	0.00191 (10.405)	—	0.871	0.109
Benchmark [Botella and Peyret (1998)]	—	0.00173	1.10979	0.864	0.112

The stability of the lid-driven cavity flow was investigated in [e.g. Poliashenko and Aidun (1995)]. For the case of a square cavity, it was reported that the point of bifurcation is $Re = 7763$, where the primary steady state becomes unstable. A range of $Re = \{0, 100, 400, 1000, 3200, 5000\}$ is considered here. The computed solution at the lower and nearest value of Re is taken to be the initial solution. The special case of $Re = 0$ starts from a fluid at rest. Ten uniform grids, namely $11 \times 11, 21 \times 21, \cdots, 101 \times 101$, are employed to study the convergence behaviour of the method. Time steps used are in the range of $0.005 - 0.5$. Steady-state solutions are presented in detail here, and they are compared with some other numerical results available in the literature.

The accuracy of the method is first examined through the solution of the Stokes flow. The governing equation for this creeping flow can be obtained from (13) by simply discarding the non-linear term and setting Re equal to 1. The computed values of the streamfunction at the centre of the primary vortex are given in Table 5. The spectral results [Botella and Peyret (1998)] are also included to provide the basis for the assessment of the accuracy of the present method. A very high degree of accuracy is achieved. When $N_{x_1} = N_{x_2} \geq 71$, five significant digits remain unchanged.

For viscous flow ($Re > 0$), results concerning the extrema of the velocity profiles along the vertical and horizontal centrelines ($Re = 100$ and $Re = 1000$), and the intensity of the primary vortex and lower right secondary vortex ($Re = 1000$) are summarized in Tables 1–4. The corresponding results obtained by the pseudospectral method [Botella and Peyret (1998)], FDM [Ghia, Ghia, and Shin (1982), Bruneau and Jouron (1990)] and FVM [Deng, Piquet, Queutey, and Visonneau (1994)] are included for comparison. The 1D-IRBFN results are in better agreement with the spectral solutions than those predicted by FDM and FVM.

For the case of $Re = 3200$ and $Re = 5000$, velocity profiles on the vertical and horizontal lines through the cavity geometric centre are plotted in Figure 2. They compare well with the corresponding results of Ghia, Ghia, and Shin (1982).

In addition, iso-vorticity lines of the flow for various Re numbers are shown in Figure 3. The vorticity-contour values chosen here are the same as those in [Ghia, Ghia, and Shin (1982), Botella and Peyret (1998)], i.e. {-5, -4,-3,-2,-1,-0.5,0,0.5,1,2,3}. The plots look reasonable when compared to those of Ghia, Ghia, and Shin (1982) and Botella and Peyret (1998).

It is worth mentioning that although the present method is global, it does not require any special treatment for the singularity at the two corners. In contrast, when using the spectral collocation method, it is necessary to employ a subtraction technique to remove the leading part of the singularity.

For the simulation of the lid-driven viscous flow, the 1D-IRBFN collocation method achieves a very high degree of accuracy using relatively coarse grids.

5 Moving interface problems

The IRBFN method is combined with the level set (LS) method in a scheme, namely IRBFN-LS, to capture the evolution of the interface. In this work, passive transport problems are chosen so that focus is kept on the moving interface.

5.1 Level set method

The underlying idea of the level set method is to embed a moving interface Γ as the zero level set of a smooth (at least Lipchitz continuous) function $\phi(\mathbf{x}, t)$ known as the level set function [e.g. Osher and Sethian (1988)]. The moving interface is then captured at all time by locating the set of $\Gamma(t)$ for which ϕ vanishes. The level set function is advected with time by a transport equation which is known as a level set equation. Usually, ϕ is defined as a signed distance function to the interface. Readers are referred to [e.g. Sethian (1999), Osher and Fedkiw (2003)] for detailed discussions on the level set method.

In the level set method, the moving interface $\Gamma(t)$ which bounds an open region $\Omega \subset \mathbf{R}^d$ ($d = 2, 3$) is embedded as the zero level set of a higher dimen-
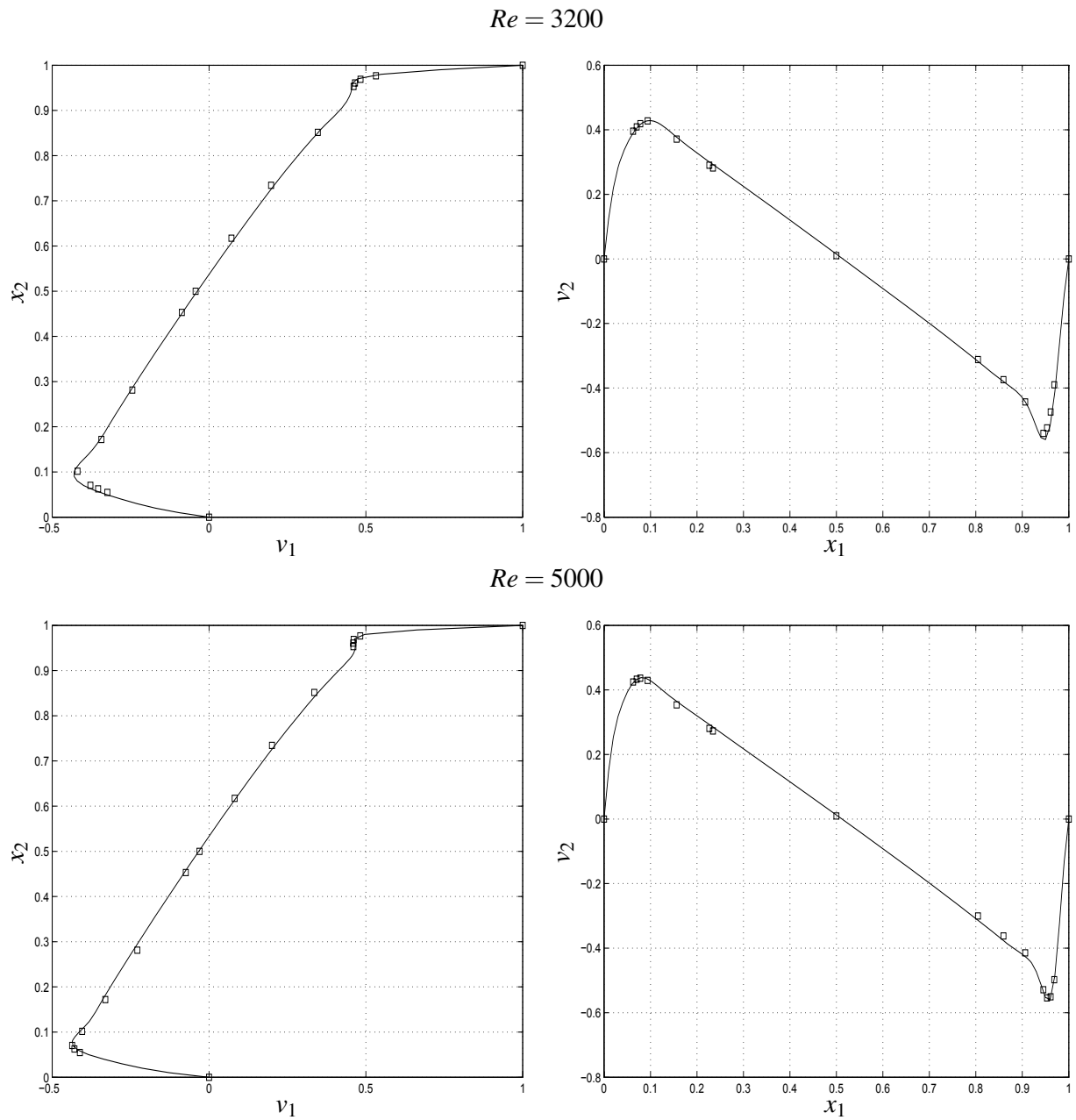
Re = 3200

Re = 5000

Figure 2: Lid-driven cavity flow, 101×101 uniform grid: Velocity profiles along the vertical and horizontal centrelines for two high values of the Reynolds number. The symbol □ denotes the corresponding results of Ghia, Ghia, and Shin (1982).

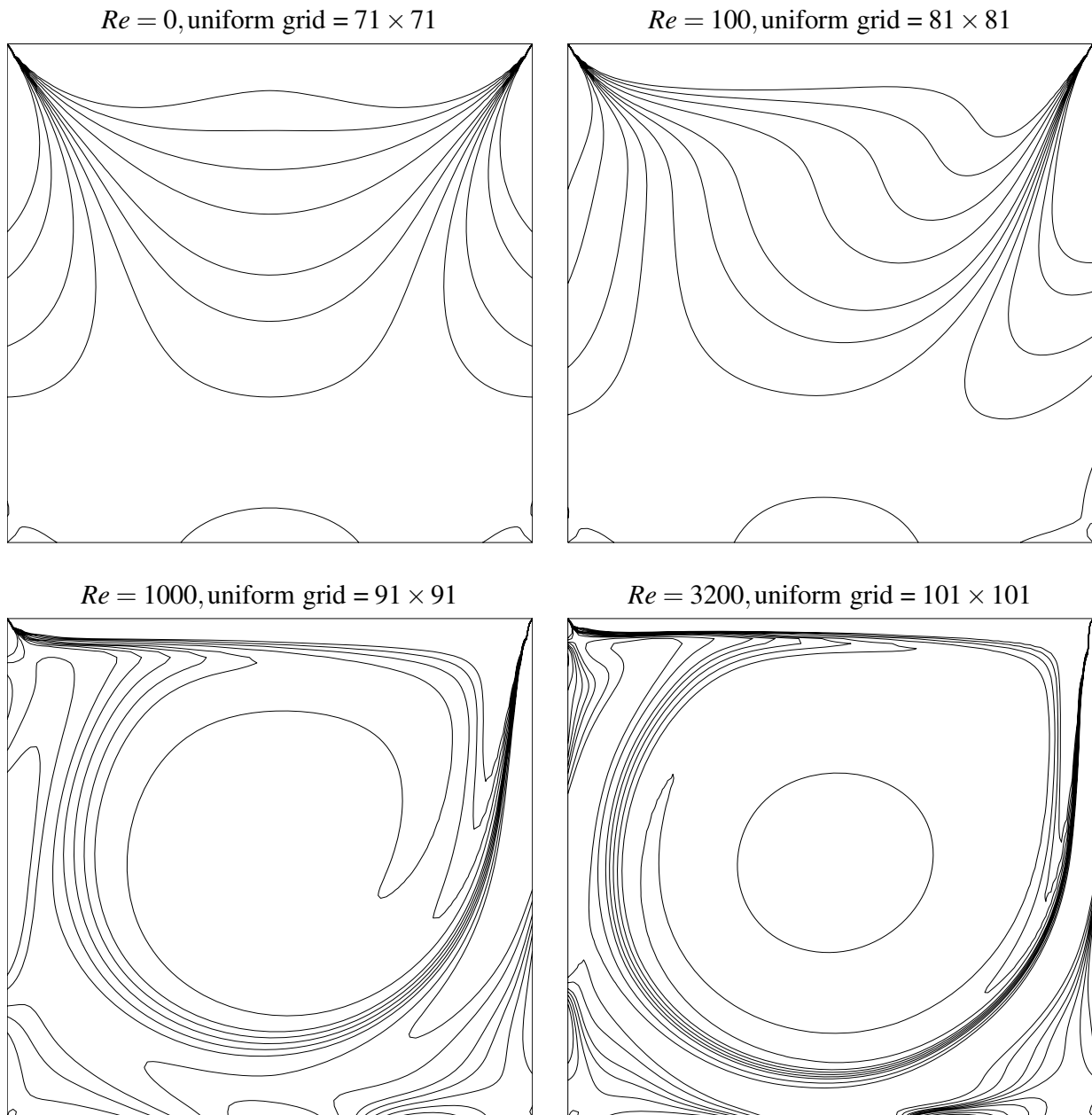$Re = 0$, uniform grid $= 71 \times 71$

$Re = 100$, uniform grid $= 81 \times 81$

$Re = 1000$, uniform grid $= 91 \times 91$

$Re = 3200$, uniform grid $= 101 \times 101$

Figure 3: Lid-driven cavity flow: Iso-vorticity lines of the flow for various *Re* numbers. The vorticity-contour values chosen here are the same as those in [Ghia, Ghia, and Shin (1982), Botella and Peyret (1998)], i.e. {-5, -4,-3,-2,-1,-0.5,0,0.5,1,2,3}.

Table 5: Lid-driven cavity flow, $Re = 0$: The minimum value of the streamfunction and its location.

Density	ψ_{min}	x_1	x_2
11×11	-0.10076	0.500	0.764
21×21	-0.10032	0.500	0.765
31×31	-0.10016	0.500	0.765
41×41	-0.10012	0.500	0.765
51×51	-0.10010	0.500	0.765
61×61	-0.10009	0.500	0.765
71×71	-0.10008	0.500	0.765
81×81	-0.10008	0.500	0.765
81×81	-0.10008	0.500	0.765
91×91	-0.10008	0.500	0.765
101×101	-0.10008	0.500	0.765
Benchmark	-0.10008	—	—
[Botella and Peyret (1998)]			

sional function $\phi(\mathbf{x}, t)$

$$\Gamma(t) = \{\mathbf{x} \in \mathbf{R}^d | \ \phi(\mathbf{x}, t) = 0\}.$$

Initially, ϕ is defined as the signed distance function from the front such that

$$\phi(\mathbf{x}, t) = \begin{cases} +d(\mathbf{x}, t) & \mathbf{x} \in \Omega^+, \\ 0 & \mathbf{x} \in \Gamma, \\ -d(\mathbf{x}, t) & \mathbf{x} \in \Omega^-, \end{cases} \qquad (21)$$

where $d(\mathbf{x}, t)$ represents the Euclidean distance from $\mathbf{x}$ to the interface, Ω^- and Ω^+ are interior and exterior regions, respectively. The interface can be then captured at any time by locating the set of $\Gamma(t)$ for which ϕ vanishes. In other words, instead of working with the interface, one evolves the level set with the following transport equation for ϕ,

$$\phi_t + \mathbf{v} \cdot \nabla\phi = 0, \qquad (22)$$
$$\phi(\mathbf{x}, 0) = \phi_0, \qquad (23)$$

where ϕ_0 is a given function. Whenever needed, the moving interface can be extracted as the zero level of the level set function ϕ. Interested readers are referred to [e.g. Osher and Sethian (1988), Sethian (1999), Osher and Fedkiw (2003)] for further details.

5.2 IRBFN-LS scheme

Consider a two-dimensional material interface moving with an externally generated velocity field. The IRBFN-LS scheme for capturing the interface is described by the following steps

1. Initialize the level set function $\phi(\mathbf{x})$ to be the signed distance to the interface as described by equation (21);

2. Update the externally generated velocity field using the current value of the level set function. For Newtonian fluid flows, this involves solving the Navier-Stokes equations by methods such as the one is discussed in section 2. For passive transport problems, the external velocity field simply remains unchanged;

3. Solve the level set equation (22) by the method of lines for one time step using the newly updated velocity field from step 2;

4. Re-initialize the level set function that has just been calculated from the previous step to a signed distance function;

5. The interface as the zero contour of the level set function has now been advanced one time step. Go back to step 2 for further evolution of the moving interface until the predefined time is reached.

5.3   Initialization

At time $t = 0$, the signed distance function in (21) is defined as the distance from the given collocation point $\mathbf{x}$ to the initial interface curve and the sign is chosen to be positive if the point is inside the curve, and negative if outside:

$$d(\mathbf{x},0) = \pm min\|\mathbf{x} - \mathbf{x}^{(i)}\|, \quad \mathbf{x}^{(i)} \in \Gamma_0, \qquad (24)$$

where $\Gamma_0 = \Gamma(0)$ is the initial interface whose discrete representation is $\mathbf{x}^{(i)}$.

5.4   Method of lines

The level set equation is solved in the IRBFN framework. Using the method of lines, one can convert the PDE (22) into a first-order initial-value system of ODEs. Spatial derivatives, i.e. $\partial \phi / \partial x_j$, are discretized by means of 2D-IRBFNs. Solving the obtained ODE system with the initial conditions (23) yields the level set function at every data point within the time interval of interest.

5.5   Re-initialization

While the level set function ϕ is initialized as a signed distance function from the moving interface, this is not necessarily true as time proceeds. In order to keep the numerical solution accurate, one needs to reinitialize ϕ to be the signed distance function from the evolving front Γ at each time step. The basic idea behind this scheme of re-initialization is that given a function $\overline{\phi}(\mathbf{x})$ that is not a distance function, one can evolve it into a function ϕ that is exact signed distance function from the zero level set of $\overline{\phi}(\mathbf{x})$ [e.g. Sussman, Smereka, and Osher (1994)]. This is accomplished by solving the following problem to steady state

$$\phi_t = S_\varepsilon(\overline{\phi})\,(1 - |\nabla \phi|) \qquad (25)$$
$$\phi(\mathbf{x},0) = \overline{\phi}(\mathbf{x}), \qquad (26)$$

where S_ε denotes the smoothed sign function

$$S_\varepsilon(\overline{\phi}) = \frac{\overline{\phi}}{\sqrt{\overline{\phi}^2 + \varepsilon^2}}, \qquad (27)$$

where ε can be chosen to be the minimum distance from any data point to the others.

The solution procedure for (25)-(27) is similar to that of (22)-(23). It should be noted that because the level set function is reinitialized at each time step, the steady solution of (25) can be obtained after just a small number of iterations [e.g. Sussman, Smereka, and Osher (1994)].

5.6   Numerical examples

5.6.1   Solid body rotation

Consider the solid body rotation of a circular bubble of radius $r = 1$ centered at $(-1,0)$ in a vortex flow with velocity field $(v_1, v_2) = (-x_2, x_1)$. A half cycle of rotation is performed, and the percentage change in area of the circle during its motion is measured. As can be seen from Table 6, the meshless IRBFN-LS scheme yields more accurate solutions with coarser point density in comparison with the mesh-based level set method [Sethian (1999)]. Figure 4 shows the zero contours of the level set function at different points in time during the rotation of the circle. In this figure, the computational grid consists of 41×41 collocation points and the time step size is chosen to be 0.0125. As can be seen from the figure, the moving interface is well captured and reconstructed by the IRBFN-LS method.

5.6.2   Circular bubble moving in shear flow

Consider a circular bubble of radius $r = 0.15$, initially centered at $(0.5, 0.7)$ moving by a shear flow in a cavity of size $[0,1] \times [0,1]$ with the velocity field (v_1, v_2) defined as follows

$$v_1 = -\sin(\pi x_1)\cos(\pi x_2), \qquad (28)$$
$$v_2 = \cos(\pi x_1)\sin(\pi x_2). \qquad (29)$$

With such velocity field, the bubble is passively transported in forms of rotation and stretching. The IRBFN-LS scheme is used to capture the moving interface with time in a computational grid of 65×65. The time step size Δt in the semi-discrete scheme for solving the level set equation is chosen following the multidimensional CFL condition [Osher and Fedkiw (2003)]

$$\Delta t \, max \left(\frac{|v_1|}{\Delta x_1} + \frac{|v_2|}{\Delta x_2} \right) = \alpha \qquad (30)$$

Table 6: Solid body rotation: Comparisons between the mesh-based LSM [Sethian (1999)] and the IRBFN-LS method on the percentage change in area at $t = 1$.

Grid size	1st-order mesh-based LSM	2nd-order mesh-based LSM	IRBFN-LS
21×21	51.88%	18.00%	1.6275%
41×41	37.981%	2.276%	0.3987%
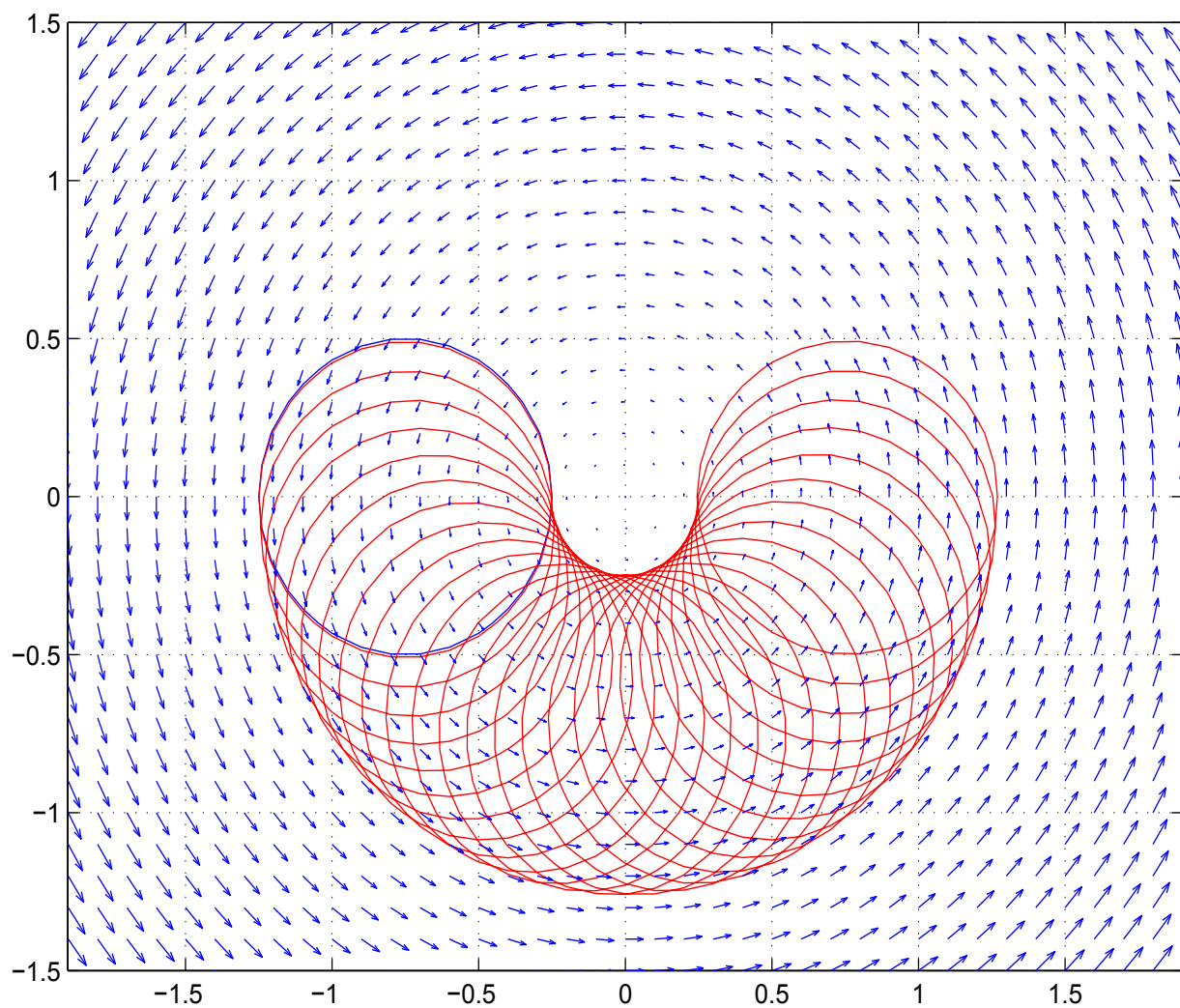
Figure 4: Solid body rotation: Zero contour of the level set function at different points in time during the rotation of a circle.
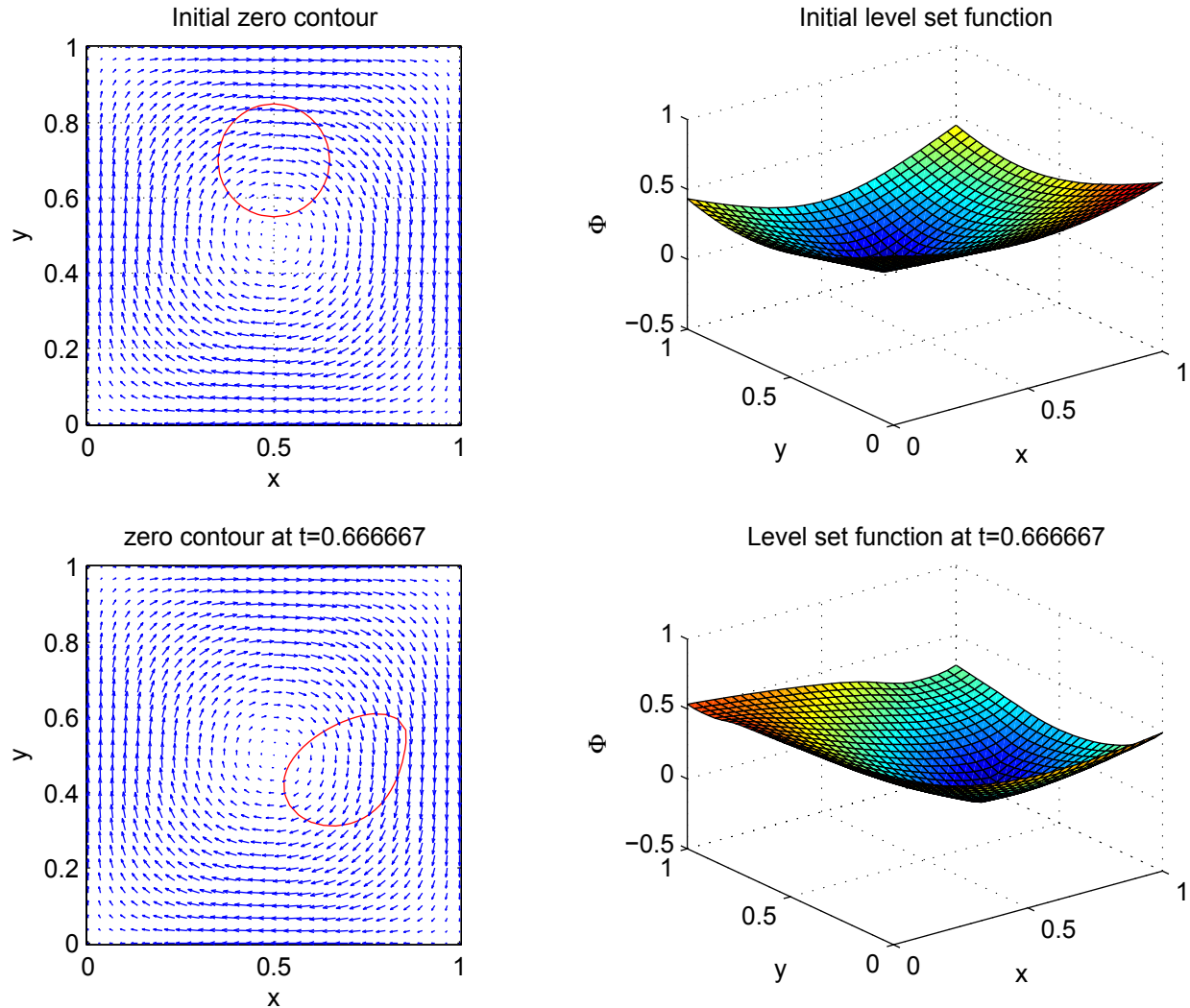
Figure 5: Circular bubble moving in shear flow: Zero contour and the level set function at $t = 0$ and $t = 0.666667$ during the rotation of a circle.

where α is the CFL number, $0 < \alpha < 1$ and $\alpha = 0.5$ for this example; $|v_1|$ and $|v_2|$ are the absolute values of normal and tangential velocity; Δx_1 and Δx_2 are grid density in the x_1- and x_2- directions, respectively. In this example, the time step size is 0.0078125. Figure 5 shows the level set function and the moving interface as its zero level at different points in time during the rotation of the circle. Reinitialization is performed after each time step with 5 iterations for the level set function to be a signed distance function. Numerical experiments are carried out with the number of steps greater than 1 where the reinitialization process is performed, and it is found that, although more computational work is needed, reinitializa-

tion after each time step yields more stable results.

6 Concluding remarks

This paper presents further developments of the IRBFN method for the simulation of viscous fluid flow problems. For the lid-driven cavity flow problem, numerical results obtained show that the method yields a very high degree of accuracy. The IRBFN results are in better agreement with the benchmark spectral solutions than those of the FDM by Ghia, Ghia, and Shin (1982). One advantage of the present method over the pseudospectral method is that it does not require any special treatment for the singularity at the two
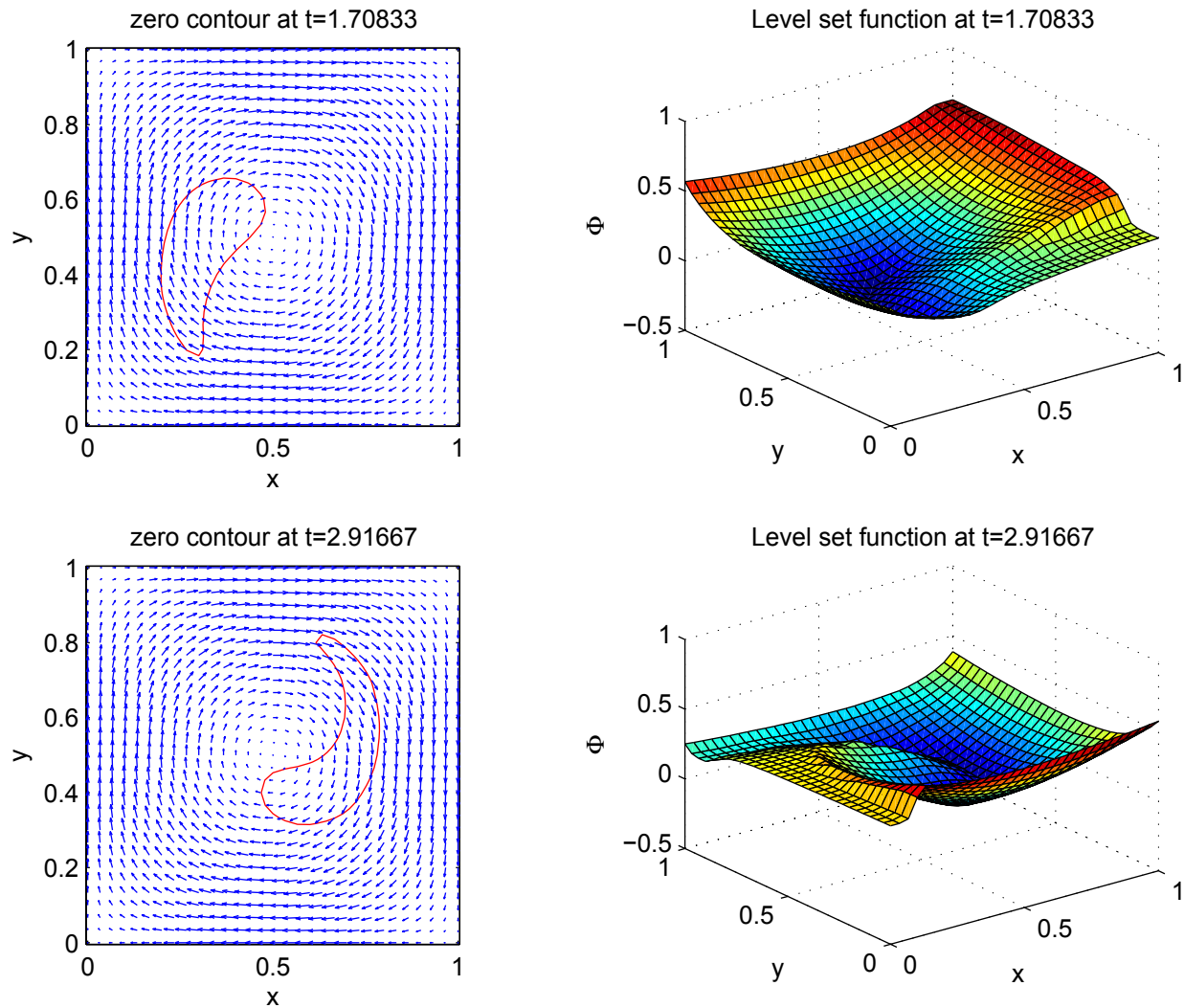
Figure 6: Circular bubble moving in shear flow: Zero contour and the level set function at $t = 1.70833$ and $t = 2.91667$ during the rotation of a circle.

top corners. For moving interface problems, the present scheme combines the highly accurate approximator coming from the IRBFN method with the advantage of the level set method in dealing quite naturally with the moving interface as the zero contour of a smooth function. It can be seen from the examples that the evolution of the moving interface is captured very well by the present scheme.

References

Botella, O.; Peyret, R. (1998): Benchmark spectral results on the lid-driven cavity flow. *Computers & Fluids*, vol. 27, pp. 421–433.

Bruneau, C.-H.; Jouron, C. (1990): An efficient scheme for solving steady incompressible Navier-Stokes equations. *Journal of Computational Physics*, vol. 89, pp. 389–413.

Chantasiriwan, S. (2006): Performance of multiquadric collocation method in solving lid-driven cavity flow problem with low Reynolds number. *CMES: Computer Modeling in Engineering & Sciences*, vol. 15, pp. 137–146.

Deng, G.; Piquet, J.; Queutey, P.; Visonneau, M. (1994): Incompressible flow calculations with a consistent physical interpolation finite volume approach. *Computers & Fluids*, vol. 23, pp. 1029–1047.

Fletcher, C. (1984): *Computational Galerkin Methods*. Springer-Verlag, New York.

Floryan, J.; Rasmussen, H. (1989): Numerical Methods for Viscous Flows with Moving Boundary. *Applied Mechanics Reviews*, vol. 42, pp. 323–341.

Ghia, U.; Ghia, K.; Shin, C. (1982): High-Re solutions for incompressible flow using the Navier-Stokes equations and a multigrid method. *Journal of Computational Physics*, vol. 48, pp. 387–411.

Hon, Y.; Ling, L.; Liew, K. (2005): Numerical analysis of parameters in a laminated beam model by radial basis functions. *CMC: Computers, Materials & Continua*, vol. 2, pp. 39–50.

Kansa, E. (1990): Multiquadrics- A scattered data approximation scheme with applications to computational fluid-dynamics-II. Solutions to parabolic, hyperbolic and elliptic partial differential equations. *Computers and Mathematics with Applications*, vol. 19, pp. 147–161.

La-Rocca, A.; Power, H.; La-Rocca, V.; Morale, M. (2005): A meshless approach based upon radial basis function hermite collocation method for predicting the cooling and the freezing times of foods. *CMC: Computers, Materials & Continua*, vol. 2, pp. 239–250.

Mai-Cao, L.; Tran-Cong, T. (2005): A Meshless IRBFN-Based Method for Transient Problems. *CMES: Computer Modeling in Engineering & Sciences*, vol. 7, pp. 149–171.

Mai-Duy, N. (2004): Indirect RBFN method with scattered points for numerical solution of PDEs. *CMES:Computer Modeling in Engineering & Sciences*, vol. 6, pp. 209–226.

Mai-Duy, N.; Tran-Cong, T. (2001a): Numerical solution of differential equations using mul-tiquadric radial basis function networks. *Neural Networks*, vol. 14, pp. 185–199.

Mai-Duy, N.; Tran-Cong, T. (2001b): Numerical solution of Navier-Stokes equations using multiquadric radial basis function networks. *International Journal for Numerical Methods in Fluids*, vol. 37, pp. 65–86.

Mai-Duy, N.; Tran-Cong, T. (2003): Approximation of function and its derivatives using radial basis function networks. *Applied Mathematical Modelling*, vol. 27, pp. 197–220.

Mai-Duy, N.; Tran-Cong, T. (2005): An efficient indirect RBFN-based method for numerical solution of PDEs. *Numerical Methods for Partial Differential Equations*, vol. 21, pp. 770–790.

Osher, S.; Fedkiw, R. (2003): *Level Set Methods and Dynamic Implicit Surfaces, Applied Mathematical Sciences (Vol 153)*. Springer, New York.

Osher, S.; Sethian, J. (1988): Fronts propagating with curvature-dependent speed: algorithms based on Hamilton-Jacobi formulations. *Journal of Computational Physics*, vol. 79, pp. 12–49.

Poliashenko, M.; Aidun, C. (1995): A direct method for computation of simple bifurcations. *Journal of Computational Physics*, vol. 121, pp. 246–260.

Sarler, B. (2005): A radial basis function collocation approach in computational fluid dynamics. *CMES: Computer Modeling in Engineering & Sciences*, vol. 7, pp. 185–194.

Sethian, J. (1999): *Level Set Methods and Fast Marching Methods: Evolving Interfaces in Computational Geometry, Fluid Mechanics, Computer Vision, and Materials Science*. Cambridge University Press, New York.

Shu, C.; Ding, H.; Yeo, K. (2005): Computation of incompressible navier-stokes equations by local RBF-based differential quadrature method. *CMES: Computer Modeling in Engineering & Sciences*, vol. 7, pp. 195–206.

Sussman, M.; Smereka, P.; Osher, S. (1994):
A level set approach for computing solutions to
incompressible two-phase flow. *Journal of Computational Physics*, vol. 114, pp. 146–159.

Tolstykh, A.; Shirobokov, D. (2005): Using radial basis functions in a "finite difference
mode". *CMES: Computer Modeling in Engineering & Sciences*, vol. 7, pp. 207–222.

Young, D.; Chen, C.; Wong, T. (2005): Solution
of Maxwell's Equations Using the MQ Method.
CMC: Computers, Materials & Continua, vol. 2,
pp. 267–276.